Interface reconstruction method for multiphase flows in under-resolved regions

Anirudh Asuri Mukundan, Thibaut Ménard, Alain Berlemont, Jorge César Brändle de Motta

Tenth International Conference on Computational Fluid Dynamics (ICCFD10), Barcelona,Spain, July 9-13, 2018

ICCFD10-2018-013

Interface reconstruction method for multiphase flows in under–resolved regions

Anirudh Asuri Mukundan[†,*], Thibaut Ménard[*], Alain Berlemont[*] and Jorge César Brändle de Motta[*]
[†]Corresponding author: anirudh.mukundan@coria.fr

[*]CNRS UMR 6614–CORIA, 76801 Saint Étienne du Rouvray, Rouen, France.

Abstract: This paper presents an interface reconstruction method called moment of fluid (MOF) method for two-phase flows using statistical moments of liquid volume fraction. In each flow solver grid cell, the liquid volume fraction and liquid center of mass are used for computing the interface unit normal. The transport of the liquid volume fraction and center of mass is performed by a directionally split advection scheme. This method is validated, results are compared with those from coupled level set volume of fluid (CLSVOF) method for 2D and 3D test cases, and is found to be at least second–order accurate in spatial resolution. Furthermore, MOF method is shown to outperform CLSVOF method in terms of interface reconstruction for thin and under–resolved liquid ligaments and filaments thereby conserving mass in the domain.

Keywords: moment of fluid, volume fraction, atomization, center of mass.

1 Introduction

Atomization of liquid fuel plays a crucial role in its subsequent combustion and pollutant formation. Due to the multiphase and multi–physical aspect of this atomization process, experimental investigations prove to be challenging endeavor. This motivates the development of numerical models and methods to study this process. An obvious requirement of these methods is least numerical error which will make it more trustable and suitable to be used in detailed simulations such as direct numerical simulations (DNS) of liquid fuel jet atomization [1–3]. In addition, these numerical methods ideally must require less computational resources, thus not taxing even the most powerful supercomputers available today [4].

Numerical simulations are powerful tools for investigation of physical processes, for example atomization. The main challenge in numerical simulations is accurately simulating the complex, turbulent, and multiphase atomization process since the two phases can have different material properties. In particular, the density ratio between the liquid and gas phases can be as high as 2000. The bottleneck with such conditions in numerical simulations is the discretization of the Navier–Stokes equations. Additionally, a force due to surface tension is generated due to the curvature of the interface that is acting only on the interface. The computation of this force can be difficult as the information about interface curvature is a prerequisite. Lastly, the accurate liquid/gas interface reconstruction method in such multiphase flows is a big challenge and has been one of the main topics of extensive research in the numerical atomization research community. Of these challenges in numerical simulations of multiphase flows, this work addresses to the development of accurate liquid/gas interface reconstruction method. Particularly, the method presented in this paper is intended specifically for reconstruction of under–resolved interface topologies such as liquid ligaments and filaments. Such interface topological structures are of importance in primary atomization simulations because mass loss in the system can occur if their interfaces are not reconstructed accurately.

Many interface capturing methods have been developed over the past decades, the prominent method being volume of fluid (VOF) method [5–8]. The predominant usage of this method comes from its inherent volume conservation property when reconstructing the interface. An implicit representation of the interface came with the level set (LS) method [9–11] which reconstructs the interface as a signed distance function

but suffered from the volume and mass losses of the phases in under–resolved flow regions. Thus, a coupled level set volume of fluid (CLSVOF) method [1, 12, 13] had been developed as an improvement to these two methods thereby combining the advantages of volume conservation and accurate interface reconstruction. Further improvements in the past years, to state a couple include, the development of consistent mass and momentum fluxes computation [14] and development of unsplit interface advection methods [13, 15].

Although these improved methods have proved to be useful in simulating multiphase flows, they can still fail in the computation of geometrical properties especially for under–resolved interface topologies. To address this limitation, moment of fluid (MOF) method [16] has been developed in the in–house code ARCHER [1, 9, 14] and presented in this work. MOF method has been proved – to preserve the orientation of the liquid/gas interface in the context of multiphase flows [16, 17]; to be second–order accurate in spatial resolution [18]. In this work, the MOF method is tested for its ability to capture under–resolved topological structures, thereby avoiding loss of mass in the system, in the context of numerical study of liquid jet primary breakup.

This paper is structured as follows. A brief description of the numerics of MOF method is presented in Section 2. This is followed by the presentation of the finite difference incompressible momentum solver used in this work along with the presentation of various numerical schemes involved in discretization of convective and diffusive terms in the Navier–Stokes equations in Section 3. The results obtained from MOF and CLSVOF methods are presented and compared in Section 4 for academic test cases in which velocity profile is imposed (Section 4.1) and in which Navier–Stokes equations are solved (Section 4.2) for the flow field and pressure. Finally, Section 5 draws the important conclusions from the results presented in this work.

2 Moment of Fluid (MOF) method

MOF method is an extension of VOF method for interface tracking in the context of multiphase flows. VOF method uses only liquid volume fraction F (0^{th} moment of the liquid volume) in every mixed computational cell. As a step further, MOF method tracks both the liquid volume fraction and coordinates of the liquid center of mass (COM) $\underline{x}_{\text{COM}}$ (1^{st} moment of liquid volume) for the interface reconstruction in each such cell. A mixed computational cell, within this study, is defined as the cell in which $0 < F < 1$ holds. The definitions of the 0^{th} and 1^{st} moments of the liquid volume are given as

$$F = \frac{\int_{\omega} d\underline{x}}{\int_{\Omega} d\underline{x}}, \tag{1}$$

$$\underline{x}_{\text{COM}} = \frac{\int_{\omega} \underline{x} d\underline{x}}{\int_{\Omega} d\underline{x}}, \tag{2}$$

where ω is the domain of the liquid packet inside the computational cell Ω. The availability of these two parameters establishes a self-sufficiency of the required information to reconstruct the approximate interface in a cell thus, eradicating data requirement from the neighboring cells. The consequence of this property is a uniform treatment of the internal and boundary cells in the mesh thus, yielding the resolution of the interface as high as that of the computational mesh itself. With the presentation of this introduction, the numerics of interface reconstruction and advection in MOF method implemented in this work are presented below.

2.1 Interface Reconstruction

The commonly used piecewise linear interface calculation (PLIC) is employed in this work for approximating the original interface. Thus, the equation of the approximated interface in 3D is given by $ax+by+cz+d = 0$, which represents the equation of a plane. In 2D, this equation becomes the equation of a line. The unit normal $\underline{n}$ of the interface is therefore expressed as $\underline{n} = [a, b, c]^T$. The shortest distance of the interface from the cell center is characterized by the parameter d.

The interface reconstruction in MOF method is a constrained optimization problem as described in [17]

wherein $\underline{n}$ and d have to be determined simultaneously by the satisfaction of the two conditions

$$\mid F^{\text{ref}} - F^{\text{act}}(\underline{n}, d) \mid = 0, \text{ and} \tag{3}$$

$$E^{\text{MOF}}(\underline{n}, d) = \min_{\text{Eq. (3) holds}} \left\| \underline{x}^{\text{ref}}_{\text{COM}} - \underline{x}^{\text{act}}_{\text{COM}}(\underline{n}, d) \right\|_2 . \tag{4}$$

All the variables containing the superscript "ref" represents the variables pertaining to the original (reference) interface while those containing the superscript "act" represents the variables pertaining to the reconstructed (actual) interface. The explanation of these conditions is assisted through Figure 1. The shortest distance of

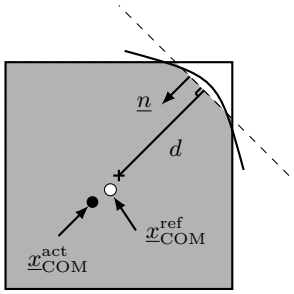

Figure 1: Pictorial representation of reference (solid line) and reconstructed (dashed line) interfaces along with liquid COM of reference (white circle) and actual (black circle) interface in a computational cell

the interface from the cell center d is determined by the volume conservation condition (c.f. Equation (3)). To this end, the linear approximated interface (shown by dashed line in Figure 1) is constructed such that liquid volume under reference (shown by solid line in Figure 1) and actual (approximated) interface is exactly the same upto the machine precision. The computation of optimal value of d is carried out using Newton–Raphson iterative method as described by Ménard et al [1]. The interface unit normal is then computed by minimizing the error E^{MOF} (also called distance defect) between the coordinates of the reference and the actual COM of the liquid in the computational cell (c.f. Equation (4)).

In order to solve this minimization problem, $\underline{n}$ is parameterized [17] using the polar coordinates as follows

$$\underline{n} = \begin{bmatrix} a \\ b \\ c \end{bmatrix} = \begin{bmatrix} \sin\Phi\cos\Theta \\ \sin\Phi\sin\Theta \\ \cos\Phi \end{bmatrix} . \tag{5}$$

Thus, the Equation (4) transforms into a non–linear least square problem for (Φ, Θ), i.e., finding (Φ^*, Θ^*) such that the error E^{MOF} is minimum, i.e.,

$$E^{\text{MOF}}(\underline{n}, d) = \left\| \underline{g}(\Phi^*, \Theta^*, d) \right\|_2 = \min_{\text{Eq.(3) holds}} \left\| \underline{g}(\Phi, \Theta, d) \right\|_2 , \tag{6}$$

where $\underline{g}(\Phi, \Theta, d) = \underline{x}^{\text{ref}}_{\text{COM}} - \underline{x}^{\text{act}}_{\text{COM}}$. Equation (6) is solved numerically for (Φ^*, Θ^*) using Gauss–Newton method. Once the optimal parametric angles (Φ^*, Θ^*) are known, the components of the unit normal $[a, b, c]^T$ can be retrieved using Equation (5). The new reference COM in each cell takes the value of the actual COM pertaining to the reconstructed interface using which the new values of the normal components are computed.

2.2 Interface Advection

The advection of interface in the case of MOF method involves advection of reference liquid volume fraction F^{ref} and coordinates of reference COM $\underline{x}^{\text{ref}}_{\text{COM}}$. A directionally split numerical scheme is employed for the advection of both quantities. The transport equation and numerical scheme implemented for the advection are presented in the following subsections. Since the advection pertains solely to the reference quantities, the superscript "ref" will be dropped in volume fraction and the coordinates of the COM hereon.

2.2.1 Volume Fraction

The advection equation for the volume fraction solved in ARCHER is given as

$$\frac{\partial F}{\partial t} + \underline{\nabla} \cdot (F\underline{u}) = c\,(\underline{\nabla} \cdot \underline{u}); \quad c = \begin{cases} 1, & F > 0.5 \\ 0, & \text{otherwise} \end{cases} \tag{7}$$

where F is the liquid volume fraction and c is a constant. A directionally split algorithm proposed in the work of Weymouth and Yue [19] is implemented for the advection of the volume fraction. For more details on the finite difference discretization of the above equation and computation of volume fluxes across cell faces, the reader is referred to [19].

2.2.2 Centre of Mass

The advection equation of the reference COM is given as

$$\frac{d}{dt}(\underline{x}_{\text{COM}}) = \underline{u}(\underline{x}_{\text{COM}}), \tag{8}$$

where $\underline{u}(\underline{x}_{\text{COM}})$ is the velocity field interpolated linearly from the face-centers of the computational cell to the location of the COM. This velocity is non–dimensionalized using the mesh spacing and the time step size $\Delta t = t^{n+1} - t^n$, hence the velocity component becomes the local Courant-Friedrichs-Lewy (CFL) number. In this study, the COM is considered as a Lagrangian particle [16, Appendix A] that is associated with a liquid packet/parcel.

An Eulerian Implicit–Lagrangian Explicit (EI–LE) scheme [20] is employed in this study for solving Equation (8). A first–order time integration of this equation keeping constant velocity over the time step size Δt yields,

$$\underline{x}^{n+1}_{\text{COM}} = \underline{x}^{n}_{\text{COM}} + u(\underline{x}^{*}_{\text{COM}}) \tag{9}$$

in which the mode of the scheme is Eulerian Implicit if $\underline{x}^{*}_{\text{COM}} = \underline{x}^{n+1}_{\text{COM}}$ and Lagrangian Explicit if $\underline{x}^{*}_{\text{COM}} = \underline{x}^{n}_{\text{COM}}$. In order to have the consistency between the advection of liquid volume fraction and COM, the mode of the scheme for COM advection is switched between EI and LE for a Cartesian direction at each time step, i.e., if $x-$direction advection of COM for $t^n \rightarrow t^{n+1}$ is carried out using EI mode, then the $x-$direction advection of COM for $t^{n+1} \rightarrow t^{n+2}$ will be carried out in LE mode. The converse is implemented for the advection along $y-$direction for the consistent advection of COM with its associated liquid packet. For the sake of completeness, the $z-$direction advection for the 3D test cases is performed in the same manner as that of $x-$direction. In this study, the coupling between the advections of the volume fraction and that of COM is carried out similar to that in the study of Jemison et al [17].

3 Coupling with momentum solver

3.1 Incompressible Navier–Stokes equations

The pressure and velocity fields describing the flow are obtained from solving the incompressible Navier–Stokes equations. The following form of the Navier–Stokes equations are solved in ARCHER:

$$\underline{\nabla} \cdot \underline{u} = 0, \tag{10}$$

$$\frac{\partial \rho \underline{u}}{\partial t} + \underline{\nabla} \cdot (\rho \underline{u}\,\underline{u}) = -\underline{\nabla} P + \underline{\nabla} \cdot (2\mu \underline{D}) + \underline{B}, \tag{11}$$

where $\underline{u}$ is the velocity field, P is the pressure field, μ is dynamic viscosity, ρ is density, $\underline{D}$ is the strain rate tensor given as $\underline{D} = \frac{1}{2}(\nabla \underline{u} + (\nabla \underline{u})^T)$, and $\underline{B}$ is the sum of the body and surface tension forces. $\underline{B} = \underline{B}_{\text{b}} + \underline{B}_{\text{st}}$ where $\underline{B}_{\text{b}}$ is the force due to gravity and $\underline{B}_{\text{st}}$ is the force due to surface tension which is given as $\underline{B}_{\text{st}} = \sigma \kappa \delta_I \underline{n}$. σ represent the surface tension, κ is the curvature of the interface computed using the liquid/gas interface unit normal $\underline{n}$ as $\kappa = \underline{\nabla} \cdot \underline{n}$, and δ_I is the Dirac delta function centered on it.

3.2 Flow solver

The solver used in this study is ARCHER, whose capabilities are described extensively in multiple works [1,9,14]. This solver is structured, parallel and developed for direct numerical simulations (DNS) of complex and turbulent multiphase flows with the application to study primary breakup of liquid fuel jet. This solver has been validated for various cases of complex turbulent flow configurations [21, 22] thus, the numerical methods employed in this solver are tailored for treating turbulence in the system.

A staggered variable configuration is used with central finite difference scheme for least numerical dissipation. One–step forward Euler and second–order total variation diminishing (TVD) Runge–Kutta schemes are available for the time advancement.

3.2.1 Projection Method

In order to solve the Equations (10) and (11), a projection method as described in Ménard et al [1] is employed. The algorithm of implementation of this method in ARCHER is given as follows:

Algorithm 1 Projection Method

1: Solve for $\underline{u}^*$:

$$\underline{u}^* = \underline{u}^n + \Delta t \left(-(\underline{u}^n \cdot \underline{\nabla})\underline{u}^n + \frac{1}{\rho^{n+1}} \underline{\nabla} \cdot (2\mu^n \underline{D}) + \frac{1}{\rho^{n+1}} \underline{B} \right) \tag{12}$$

2: Solve for pressure P^{n+1} (Poisson equation for pressure):

$$\underline{\nabla} \cdot \left(\frac{1}{\rho^{n+1}} \left(\underline{\nabla} P^{n+1} \right) \right) = \frac{\underline{\nabla} \cdot \underline{u}^*}{\Delta t} \tag{13}$$

3: Solve for $\underline{u}^{n+1}$:

$$\underline{u}^{n+1} = \underline{u}^* + \frac{\Delta t}{\rho^{n+1}} (-\underline{\nabla} P^{n+1}) \tag{14}$$

Equation (13) is obtained from the application of the divergence operator on Equation (14). The solution of the Poisson equation is essential to obtain the pressure which in turn is required in Equation (14) to solve for $\underline{u}^{n+1}$.

3.2.2 Numerical Methods

The numerical schemes used in this study for the discretization of the various terms in the Navier–Stokes equations are presented as follows. A 2^{nd} order central difference scheme is employed for discretization of the spatial derivatives to avoid any dissipation. However, the convection term is discretized using 5^{th} order WENO scheme to ensure a robust behavior of the solution. A consistent mass and momentum flux computation [14] is employed. The viscous term is discretized following the method described in Sussman et al [23]. Ghost Fluid Method (GFM) [24] is employed for the spatial discretization of the Poisson equation (Equation (13)) for taking into account the force due to surface tension as a pressure jump. The resulting linear system of symmetric and positive definite matrix with five diagonals is solved using multigrid algorithm for preconditioning a conjugate gradient (CG) method [9]. The temporal derivatives in this study are discretized using one-step forward Euler scheme.

4 Validation and numerical results

4.1 Transport and Deformation Tests

Having described the MOF method, results from various numerical tests are presented in this section to assess its accuracy, order of convergence, and utility as interface reconstruction method. The choices of these test cases are made so that the errors due to reconstruction and advection algorithms can be evaluated. In multiple

tests presented in the following subsections, the reconstruction accuracy of MOF and CLSVOF algorithms are compared along with the order of convergence of the error with respect to the spatial resolution of the mesh. The CLSVOF reconstruction algorithm of Ménard et al [1] is used for result comparison with MOF method in this work.

In all the test cases presented in this work, a constant CFL number of 0.5, periodic boundary conditions along $x-$ and $y-$directions, and $\Delta x = \Delta y$ ($= \Delta z$ in 3D) are employed. The time step size Δt is computed from the CFL number and the mesh spacing unless stated otherwise explicitly.

The quantification of the error for each test case varies and are carried out in three ways. The formula for the computation of each of the error reported in this study are given below:

$$E_{L_1} = \sum_{i,j,k} V_{i,j,k} \mid F(i,j,k,T) - F(i,j,k,0) \mid, \tag{15}$$

$$E_{nL_1} = \frac{\sum\limits_{i,j,k} \mid F(i,j,k,T) - F(i,j,k,0) \mid}{\sum\limits_{i,j,k} \mid F(i,j,k,0) \mid}, \quad \text{and} \tag{16}$$

$$E_{\text{vol}} = \Big|\sum_{i,j,k} F(i,j,k,T) - \sum_{i,j,k} F(i,j,k,0)\Big| \tag{17}$$

where F is the liquid volume fractions, $V_{i,j,k} = \Delta x \Delta y \Delta z$ is the volume of each computational cell in the mesh, and T is the physical final time until which the simulation is run. For the 2D test cases presented in this study, the $V_{i,j,k}$ becomes the area of each cell computed as $V_{i,j} = \Delta x \Delta y$.

4.1.1 Zalesak's notched disk test

First, the traditional Zalesak's notched disk test that were performed in many studies, for example [13,25,26], is presented here. In this test, a slotted circle of fluid revolves around the center of the domain in a solenoidal velocity field. Within the scope of this test, MOF and CLSVOF methods are used separately as interface reconstruction method and the results of each are compared and contrasted.

The premise of this test is as follows: a slotted circle of radius $r = 0.15$ units having slot width of 0.06 units and slot length of 0.2 units is placed in a 1×1 domain with center of the circle located at $(0.5, 0.75)$. The revolution of this slotted circle around the center of the domain is accomplished using the following velocity field

$$u = \frac{\pi}{3.14}(0.5 - y), \text{ and} \tag{18}$$

$$v = \frac{\pi}{3.14}(x - 0.5). \tag{19}$$

Since this velocity is divergence-free throughout the domain, the interface of the Zalesak's notched circular disk is expected to retain the original shape at the end of rotation. The test ends when the first (anticlockwise) revolution of the slotted circular disk is completed. The resulting error between the exact and the reconstructed interface is then computed using Equation (16).

The initial interface is depicted using black solid line, the final interface from MOF method is depicted using red solid line while that from CLSVOF method is depicted using blue solid line. It can be observed from Figures 2a to 2c, that the error in reconstruction is mainly concentrated in the regions of high curvature of the interface. Furthermore, it is obvious from from Figure 2d that the MOF method is quantitatively more accurate in capturing the interface under a solenoidal velocity field than CLSVOF method and displays second–order convergence rate in spatial resolution.

4.1.2 Vortex in a box test

A progressively more strict test for an interface capturing method is vortex in a box test. This test assesses the ability of an interface reconstruction method to represent the under–resolved interfacial structures, such as ligaments, in a robust manner. A circular disk is made to undergo severe deformation under a given

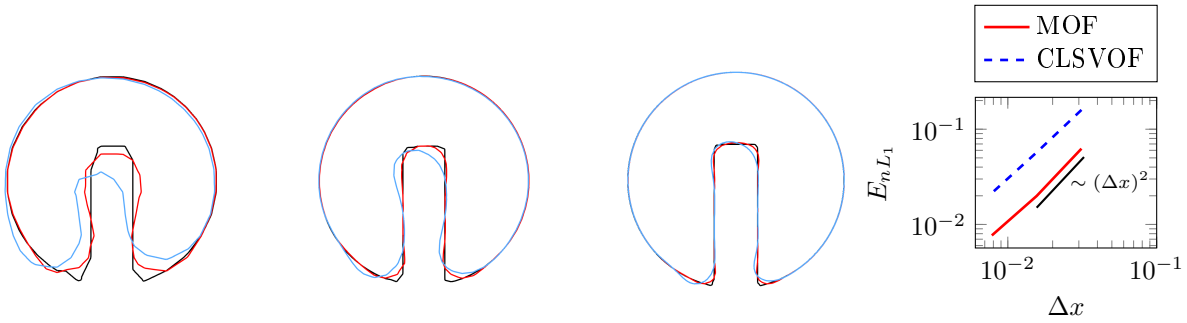

(a) 32×32 (b) 64×64 (c) 128×128 (d) Error convergence for Zalesak disk rotation

Figure 2: Initial and final interfaces of Zalesak's slotted disk after one full revolution and error convergence plot; (a)–(c): red contour line correspond to MOF; blue contour line correspond to CLSVOF; black contour line correspond to initial interface

velocity field. The following time reversing velocity field is prescribed in the 1×1 domain

$$u = -2\sin^2(\pi x)\sin(\pi y)\cos(\pi y)\cos(\pi t/T) \tag{20}$$

$$v = 2\sin^2(\pi y)\sin(\pi x)\cos(\pi x)\cos(\pi t/T) \tag{21}$$

where T is the time period of reversal of the velocity field. In this study, $T = 6$ is chosen for the analysis of the interface reconstruction accuracy. This velocity field stretches and tears the initially circular fluid body as it becomes progressively entrained by the vortex and comes back to its original shape at time $t = T$. The entrainment is demonstrated as long thin fluid filament spiraling inward towards the vortex center. Unlike Zalesak's notched disk test, the velocity field in this test is non–linear deeming this test to be a more realistic assessment for the reconstruction method.

The results of the interfaces are shown in Figure 3 for the mesh resolutions 64×64, 128×128, and 256×256 with the reference solution (depicted by black solid line in the subfigures) obtained on a 1024×1024 grid. The top row in this figure pertain to the time instant $t = T/2$ corresponding to the maximum stretching of the fluid body and those at the bottom row pertain to the time instant $t = T$ corresponding to the return to the original shape. The reconstruction algorithm proves to be robust in the smooth regions of the interface and it can be said qualitatively that the L_1-error reduces with the increase in mesh resolution at both the time instants of maximum stretch and at final time instant at which the interface returns back to its original shape. It is obvious from the top subfigure in Figure 3b that MOF method is able to capture thin ligaments at the tail of the spiral at the time instant of maximum stretch. Figure 3d quantifies the L_1-error computed at time $t = T$ when the interface returns to its initial shape. From this figure, it can be seen that both MOF and CLSVOF reconstruction algorithms are of the same level of accuracy in terms of reconstruction error. Once again, it can be seen that the MOF method exhibit second–order accuracy in spatial resolution.

4.1.3 Circular fluid body deformation test

To have even more stringent test for the MOF method, a complex time reversing velocity field [27] given by

$$u = \sin(4\pi(x + 1/2))\sin(4\pi(y + 1/2))\cos(\pi t/T) \tag{22}$$

$$v = \cos(4\pi(x + 1/2))\cos(4\pi(y + 1/2))\cos(\pi t/T) \tag{23}$$

is used in this test for the deformation of a circular liquid droplet to induce radical deformations to the interface. To this end, a circular liquid droplet of radius $r = 0.15$ units is placed with its center at $(0.5, 0.75)$ in a 1×1 domain. At its maximum deformation, the circular fluid body is entrained into two of the four nearest vortices with a small portion (thin filaments) entrapped by the two of the neighboring vortices. The time period for velocity reversal chosen is $T = 2.0$.

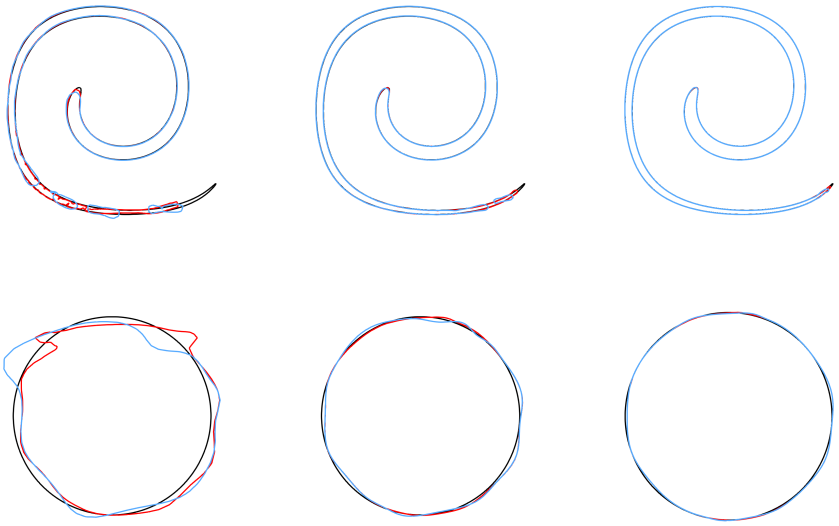

(a) 64×64 (b) 128×128 (c) 256×256

(d) Error convergence for vortex in a box test

Figure 3: Vortex in a box test; $t = T/2$ (top row) and $t = T$ (bottom row) and error convergence plot for $T = 6$; (a)–(c): red contour line correspond to MOF; blue contour line correspond to CLSVOF; black contour line correspond interface from 1024×1024 grid

The results are shown in Figures 4b to 4d for the 128×128, 256×256, and 512×512 mesh resolutions respectively for $t = T/2$ (top row) and $t = T$ (bottom row) with initial interface (black line), reconstructed interfaces using MOF (red line), and CLSVOF (blue line) for the corresponding time instants. In addition, a zoomed view of the miniature ligament found in the final time iteration for the 512×512 mesh is shown. From this zoomed view along with the underlying mesh, it can be seen that the depicted interface structure is extremely under–resolved. Thus, even with MOF method spurious oscillations in the final interface are seen in the figures in the top row of Figures 4b to 4d. Albeit this current limitation, even under extreme velocity fields which is tearing the interface apart, the MOF method is observed to perform satisfactorily for interface reconstruction under extreme deformations of the liquid body topology (c.f. top row in Figures 4b to 4d).

The plot of the convergence of the L_1-error is shown in Figure 4a for mesh resolutions ranging from 32×32 to 512×512. This error initially decreases at a slower rate and then decreases faster with increasing mesh resolution. Furthermore, it can be seen that both the MOF and CLSVOF method exhibits a third–order convergence rate for all the spatial resolutions considered for this test case. The reason for this behavior in comparison to the other test cases could be attributed to the fact that as the mesh resolution increases, particularly for this test case, smaller structures of the interface are increasingly identified thereby enhancing the convergence rate of the error.

4.1.4 Liquid spherical droplet deformation test

With the presentation of the results pertaining to 2D test cases, it is therefore interesting to assess the accuracy of MOF method for 3D test case with imposed non-linear velocity field in the domain. As an example for such a test case, deformation of three-dimensional liquid droplet is considered. This test case, was initially proposed in [28] using the velocity field described in the work of LeVeque [29], assesses the robustness and properties of convergence of the interface reconstruction method in three-dimensional configurations. Following [13], it is presented in this paper for qualitative test for the capabilities of MOF in 3D setup.

The test consists of a spherical liquid droplet of radius 0.15 placed in a $1 \times 1 \times 1$ domain with its center

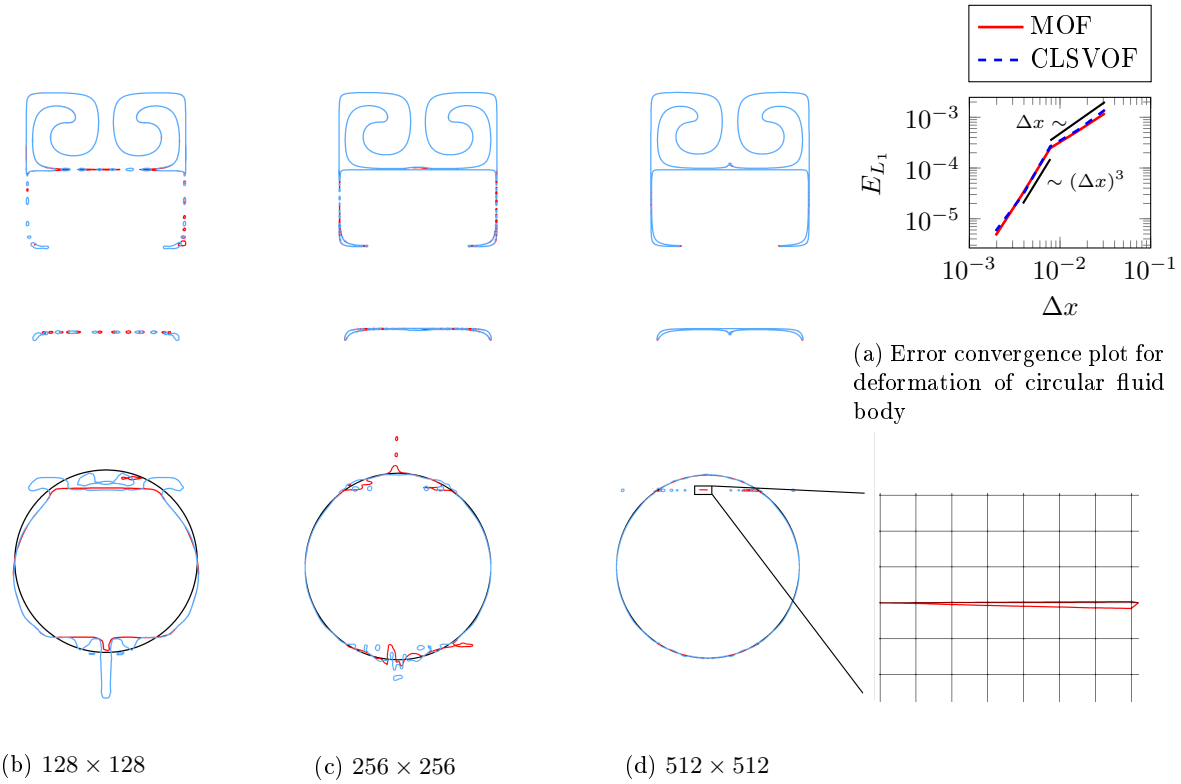

(a) Error convergence plot for deformation of circular fluid body

(b) 128×128 (c) 256×256 (d) 512×512

Figure 4: Interface reconstruction for deformation of circular fluid body $t = T/2$ (top row) and $t = T$ (bottom row) and error convergence plot using MOF method; (a)–(c): red contour line correspond to MOF; blue contour line correspond to CLSVOF; black contour line correspond to initial interface

located at $(0.35, 0.35, 0.35)$ undergoing a severe deformation under the following time reversing velocity field.

$$u(x, y, z, t) = 2\sin^2(\pi x)\sin(2\pi y)\sin(2\pi z)\cos(\pi t/T) \tag{24}$$

$$v(x, y, z, t) = -\sin(2\pi x)\sin^2(\pi y)\sin(2\pi z)\cos(\pi t/T) \tag{25}$$

$$w(x, y, z, t) = -\sin(2\pi x)\sin(2\pi y)\sin^2(\pi z)\cos(\pi t/T) \tag{26}$$

with time period of reversal of the velocity chosen to be $T = 3$. The domain is discretized using multiple mesh resolutions $64 \times 64 \times 64$, $128 \times 128 \times 128$, $256 \times 256 \times 256$, and $320 \times 320 \times 320$. The result of the simulation run for the $320 \times 320 \times 320$ mesh resolution is presented in Figures 5a to 5c for the time instants $t = 0, 1.5$, and 3 respectively. Additionally, a slice of the membrane of the sphere under extreme deformation (i.e., $t = 1.5$) is also shown in Figure 6. Three noteworthy inferences can be drawn from these results: one, there are no holes in the spherical membrane under the extreme deformation evidently conclusive of the better performance of the interface capturing by MOF method; two, even though the slice of the sphere at $t = 1.5$ is only resolved to single cell, MOF is able to perform robustly under severely deforming velocity field; and three, at final time $t = T = 3$, the shape obtained is close to the initial shape of the sphere, except for a little deformation. The computed volume error (c.f. Equation (17)) for this mesh resolution in this test case is around 6×10^{-7} which is a clear evidence of the superior capability of MOF method.

The L_1-error (c.f. Equation (15)) shown in Figure 7a initially converges slowly as a first–order and then rapidly with the second–order in spatial resolution. For the case of volume error (c.f. Equation (17)) shown in Figure 7b, the error converges rapidly at a third–order for the coarse meshes and decreases as fifth–order in spatial resolution after 256 mesh points per Cartesian direction.

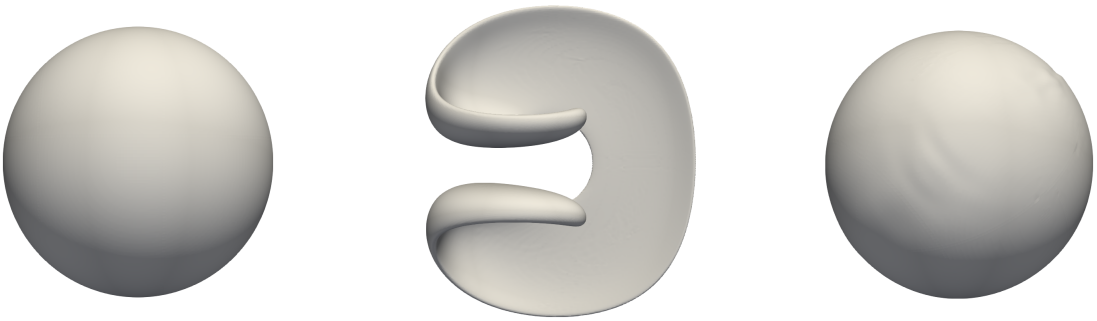

(a) $t = 0$ (b) $t = 1.5$ (c) $t = 3$

Figure 5: Interface position of a spherical liquid droplet at various time instants for $320 \times 320 \times 320$ mesh using MOF method

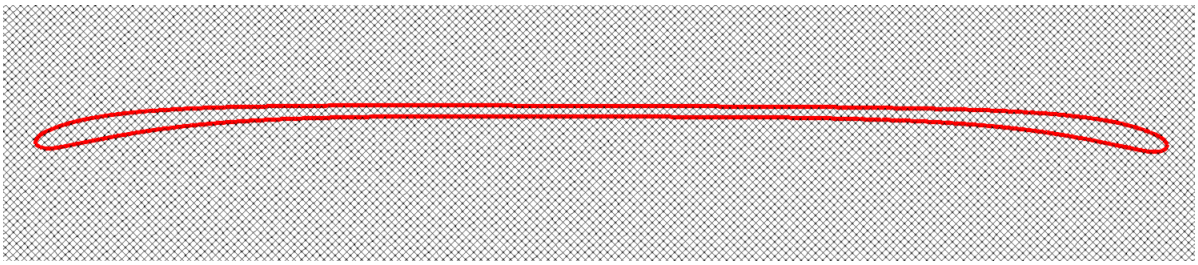

Figure 6: Slice of spherical membrane at $t = 1.5$ for spherical liquid droplet deformation for $320 \times 320 \times 320$ mesh

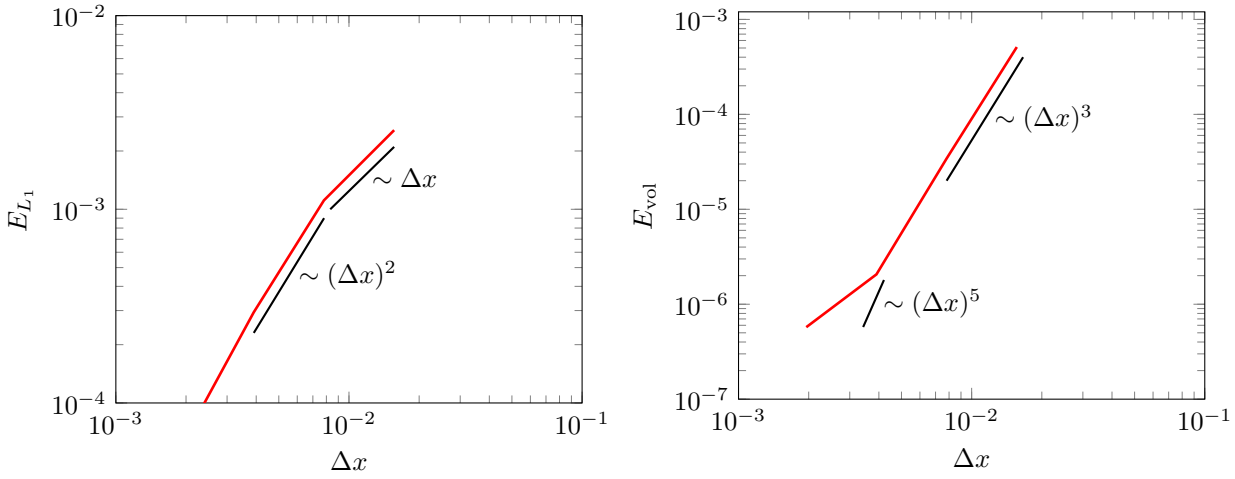

(a) L_1-error convergence plot (b) Volume error convergence plot

Figure 7: Error convergence plot for various mesh resolutions for spherical liquid droplet deformation test using MOF method

4.2 Applications

With the results of interface reconstruction for various deformative settings presented, we now focus on the application of the MOF method to problems that involve complex interface topologies coupled with solving the Navier–Stokes equations.

4.2.1 2D Shear Layer test

The MOF method is now applied to a purely convection driven physical problem of a 2D shear layer. This test was performed using CLSVOF method as interface capturing method by Vaudor [30] for testing the robustness of computation of the convection term and the computation of the mass and momentum fluxes. The conclusion was presence of unphysically high velocity values in the domain resulting from incorrect computation of mass and momentum fluxes which has its causal link to the underlying interface capturing method. It is now intriguing to perform the same test case with MOF as interface reconstruction method under such extreme convective conditions and compare the results with that of CLSVOF.

In this test case, a 2D shear layer as shown in Figure 8 is considered and placed in a $L \times L$ domain with a liquid shear layer of thickness $\delta = L/10$ and gas phase on its either sides. The value of $L = 0.003$ is chosen in this work. The gas phase flowing from left to right at a very high velocity in comparison to the liquid phase causes shear and results in atomization of the liquid shear layer. The liquid phase has density of $\rho_{\mathrm{l}} = 1000$

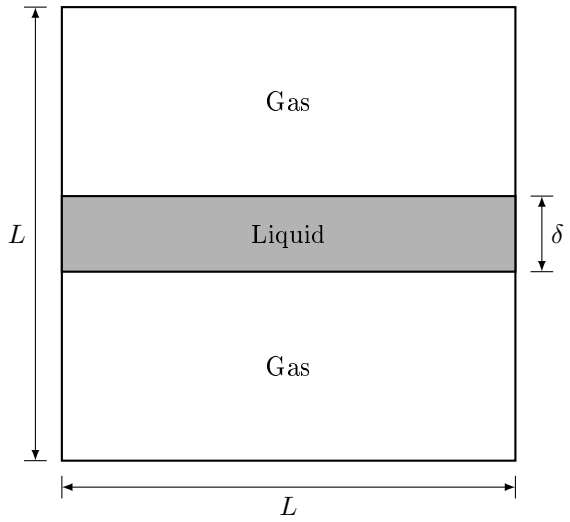

Figure 8: Configuration of a 2D shear layer test case dominated by convection

and the gas phase has a density of $\rho_{\mathrm{g}} = 1$. A divergence free initial velocity field is prescribed in the domain given as follows

$$u = A - 0.04 \cos\left(\frac{2\pi x}{L}\right)\left(\frac{L}{x}\right)\left(\frac{-2}{\delta}\right)\exp\left(-\frac{2y}{\delta}\right), \tag{27}$$

$$v = 0.04 \sin\left(\frac{2\pi x}{L}\right)\exp\left(-\frac{2y}{\delta}\right) \tag{28}$$

in which δ is the thickness of the liquid shear layer and the value for A is taken as

$$A = \begin{cases} 30\ , \text{ in gas phase} \\ 2\ , \text{ in liquid phase.} \end{cases} \tag{29}$$

Five mesh resolutions are considered in this test case ranging from 32×32 to 512×512 and periodic boundary conditions are used along $x-$ and $y-$directions. The simulation is run until the physical time $t = 3 \times 10^{-3}$.

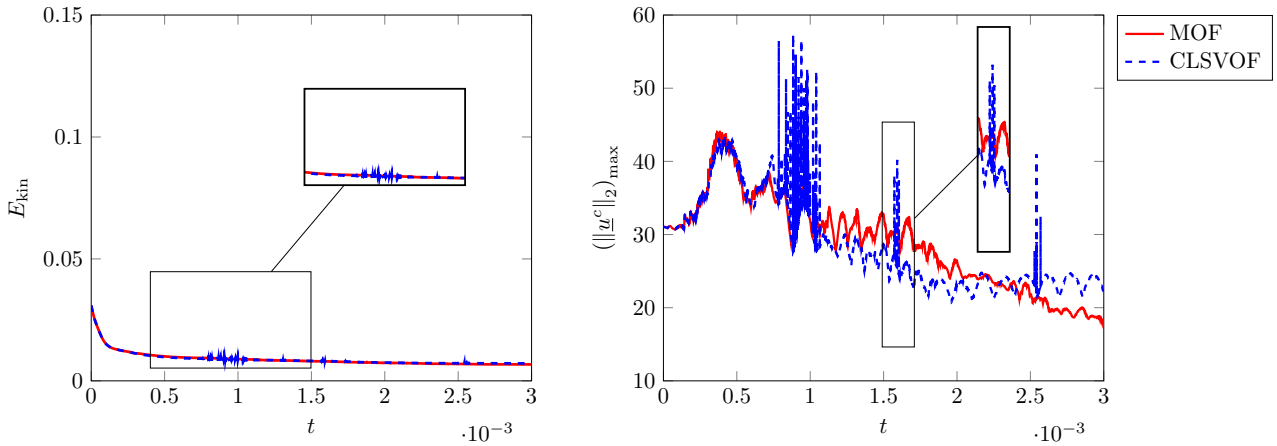

(a) Sum of kinetic energies of liquid and gas phases (b) Peak cell centered velocity magnitude in the domain

Figure 9: Time-based evolution of sum of kinetic energies of liquid and gas phases, and maximum velocity magnitude in the domain for 64×64 mesh resolution for 2D shear layer test case. Solid red line: MOF, dashed blue line: CLSVOF

Since periodic boundary conditions are used in this test case, the total kinetic energy of the system theoretically has to be preserved at all times. An additional expectation is non–presence of spurious velocity spikes for single time step. To test these two expectations, a plot of time evolution of the sum of kinetic energies of liquid and gas phases, and the evolution of maximum cell centered velocity magnitude $\|\underline{u}^c\|_2 \left(= \sqrt{(u^c)^2 + (v^c)^2}\right)$ in the domain for the 64×64 mesh resolution are shown in Figure 9.

Figure 9a shows the time evolution of the total kinetic energy computed as the sum of the kinetic energies of liquid and gas phases. The red solid line correspond to results obtained using MOF while blue dashed line using CLSVOF method in this plot. The reduction in the total kinetic energy of the system over time is caused by the numerical diffusion of the WENO scheme employed for convection term. This reduction is minor and thus essentially total kinetic energy of the system is preserved over time. However, from the inset plot in Figure 9a, it is apparent that the CLSVOF method is experiencing large number of small spikes in the total kinetic energy. This is due to the spurious velocity shoot ups in the domain when using CLSVOF method. Such shoot ups are evident from observing Figure 9b which shows the time evolution of peak of the cell centered velocity magnitude in the domain. It is seen in this plot (and in its inset plot) that there are large number of spurious velocity spikes in the domain at multiple time instants when CLSVOF is used as interface reconstruction method. However, when using MOF method, such sudden increase in the velocity is not encountered. This is due to the correct computation of the interface unit normal in MOF method thereby leading to correct computation of density resulting in accurate computation of velocity field. Thus, clearly, it is proved again that MOF is performing better than CLSVOF under the extreme convective conditions.

The visualization of this shear layer using MOF method is shown in Figure 10 for two time instants. The liquid/gas is interface represented by solid black line and the contour plot is colored using the magnitude of the cell centered velocity in the cut plane shown. It can be seen that the liquid/gas interface is getting severely distorted due to the high velocity of the gas phase even at times as early as $t = 4.9 \times 10^{-4}$. At the final time instant of $t = 3 \times 10^{-3}$, the liquid shear layer is atomized into larger droplets and ligaments.

4.2.2 Rayleigh–Taylor instability test

Finally, the MOF method is applied to the Rayleigh–Taylor instability problem which has been investigated extensively by many, for example [31–33]. However, these works did not consider effect due to surface tension. In recent studies, such as [11, 13, 26], this effect has been considered and hence, the same configuration and numerical setup will be used in this study. To be specific, this case study follows the work of Desjardins and Pitsch [26].

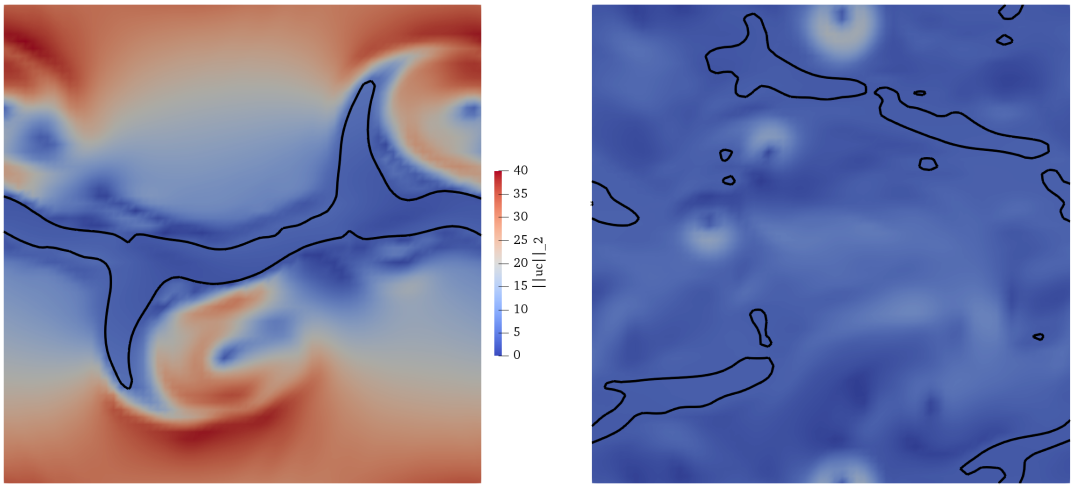

(a) $t = 4.9 \times 10^{-4}$ (b) $t = 3 \times 10^{-3}$

Figure 10: Liquid/gas interface for 2D shear layer colored by contour of magnitude of cell centered velocity for $t = 4.9 \times 10^{-4}$ and $t = 3 \times 10^{-3}$ using MOF method. Flow direction from left to right.

In this test case, a 1×4 domain is considered containing two fluid phases about each other that are separated by an interface. This interface is defined by the zero value of the level set given as

$$\phi(x, y) = y + A\cos(2\pi x) \tag{30}$$

where $A = 0.05$ is chosen for this test case. The density of the top fluid (denoted as fluid 1) is $\rho_1 = 1.225$ while that of the bottom fluid (denoted as fluid 2) is $\rho_2 = 0.1694$. The dynamic viscosities of the two fluids are same $\mu_1 = \mu_2 = 0.00313$. The surface tension is taken as $\sigma = 0.1337$. Periodic boundary condition is considered along $x-$direction and wall boundary condition along $y-$direction. Five different mesh resolutions are considered ranging from 32×128 to 512×2048. The test case is run upto a physical time of $t = 1.2$.

Figure 11 shows the interface shape as a function of time for the 512×2048 mesh resolution. These results are in good agreement with that of Desjardins and Pitsch [26] that was performed with a spectrally refined level set method.

Figure 12 shows the fluid phase interfaces for all mesh resolutions for the time steps $t = 1.0, 1.1, 1.2$. The arrow in these figures indicates the increasing mesh resolutions considered in this work for this test case.

For the quantitative assessment of the performance of MOF method for this test, an error defined as the difference between maximum penetration of the spike of the fluid 1 into fluid 2 is computed for each mesh resolution considering the finest as the reference solution. This spike penetration error is plotted as a function of the mesh resolution and is shown in Figure 13 for time instants $t = 1.0, 1.1, 1.2$. Three inferences are to be noted at this juncture: first, it can be observed that the trend of the error convergence in the plot is in very good agreement with that from Desjardins and Pitsch [26]; second, the error initially converges at a slower rate and then rapidly increases to third-order in spatial resolution; and third, the error convergence reverts back to first-order after the 128×256 mesh resolution which could be attributed to the formation of smaller and complex topological structures with large curvature as the time proceeds.

5 Conclusions

Study of liquid fuel atomization process is essential in order to meet the stringent emission norms. This is due to the fact that this process has a direct influence on the production of pollutant emissions. Numerical study of atomization under turbulent conditions give insights which are otherwise challenging to obtain through

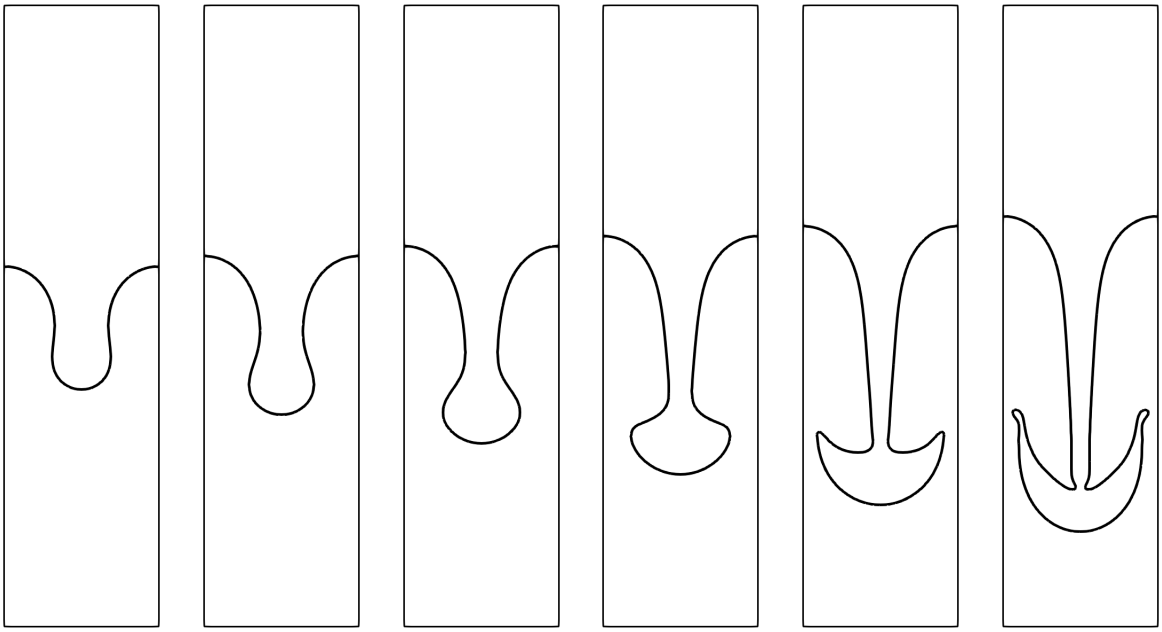

(a) $t = 0.7$ (b) $t = 0.8$ (c) $t = 0.9$ (d) $t = 1.0$ (e) $t = 1.1$ (f) $t = 1.2$

Figure 11: Fluid phase interface shape as a function of time for 512×2048 mesh resolution using MOF method

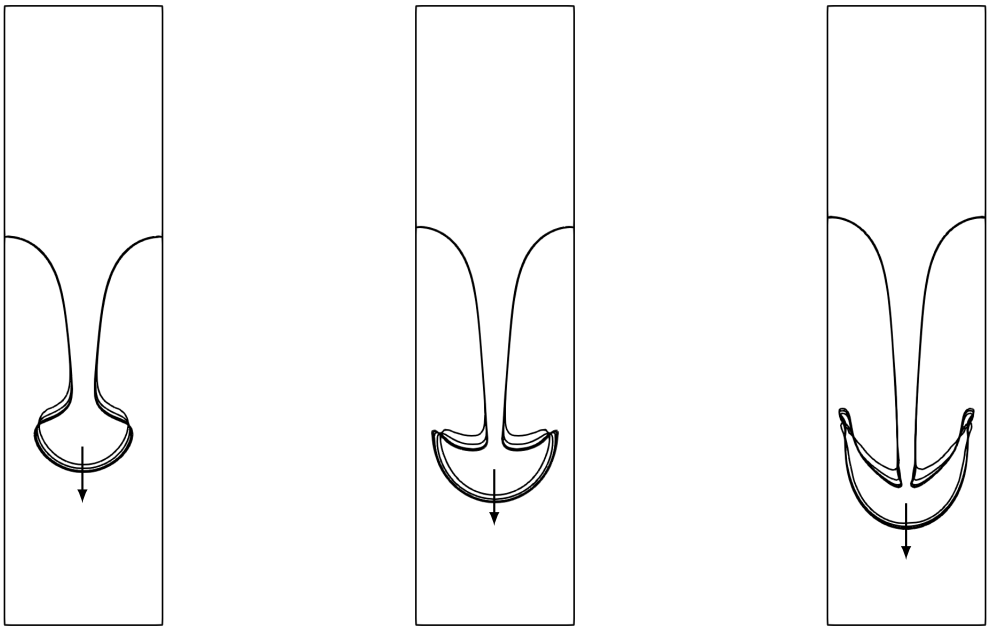

(a) $t = 1.0$ (b) $t = 1.1$ (c) $t = 1.2$

Figure 12: Fluid phase interface shape as a function of time for Rayleigh–Taylor instability test using MOF method with arrow indicating increasing mesh resolutions from 32×128 to 512×2048

experimental investigations.

In this work, the moment of fluid (MOF) method was presented for liquid/gas interface reconstruction in the context of incompressible multiphase flows to the application of numerical analysis of primary breakup

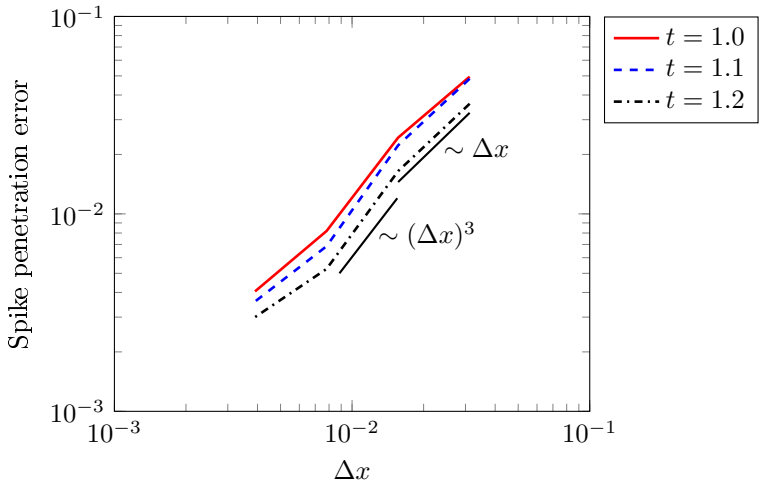

Figure 13: Error convergence plot for various mesh resolutions for Rayleigh–Taylor instability test considering 512×2048 mesh as reference solution using MOF method

of liquid fuel. In this method, the unit normal of the liquid/gas interface is computed by reducing the defect in the first order moment of liquid volume, i.e., coordinates of liquid center of mass, in a volume conservative manner. For various test cases presented in this study, MOF method proved to be at least as accurate as that of CLSVOF method in terms of reconstruction error, preservation of the shape, and orientation of the interface topologies. Moreover, MOF method demonstrated its superior capability of preserving the interface for under–resolved topological structures such as thin filaments and ligaments. Furthermore, this new method of interface reconstruction has proved to avoid spurious unphysical velocity for such topologies and produce nearly third-order convergence error when coupled with Navier–Stokes equations. This deems MOF method a robust and accurate interface reconstruction method that can be used in DNS of primary atomization.

Acknowledgements

The funding for this project from the European Union's Horizon 2020 research and innovation programme under the Marie Skłodowska-Curie grant agreement N° 675676 is gratefully acknowledged. The computing time at CRIANN (Centre Régional Informatique et d'Applications Numériques de Normandie) under the scientific project No. 2003008 is also gratefully acknowledged.

References

[1] T. Ménard, S. Tanguy, and A. Berlemont. Coupling level set/VOF/ghost fluid methods: Validation and application to 3D simulation of the primary break-up of a liquid jet. *International Journal of Multiphase Flow*, 33(5):510–524, 2007.

[2] O. Desjardins and H. Pitsch. Detailed numerical investigation of turbulent atomization of liquid jets. *Atomization and Sprays*, 20(4):311–336, 2010.

[3] V. Le Chenadec and H. Pitsch. A conservative framework for primary atomization computation and application to the study of nozzle and density ratio effects. *Atomization and Sprays*, 23(12):1139–1165, 2013.

[4] M. Gorokhovski and M. Herrmann. Modeling primary atomization. *Annual Review of Fluid Mechanics*, 40:343–366, January 2008.

[5] E. Aulisa, S. Manservisi, R. Scardovelli, and S. Zaleski. A geometrical area-preserving volume-of-fluid advection method. *Journal of Computational Physics*, 192(1):355–364, 2003.

[6] J. López, C. Zanzi, P. Gómez, F. Faura, and J. Hernández. A new volume of fluid method in three dimensions–Part II: Piecewise-planar interface reconstruction with cubic-Bézier fit. *International Journal for Numerical Methods in Fluids*, 58(8):923–944, 2008.

[7] J. Hernández, J. López, P. Gómez, C. Zanzi, and F. Faura. A new volume of fluid method in three dimensions–Part I: Multidimensional advection method with face-matched flux polyhedra. *International Journal for Numerical Methods in Fluids*, 58:897–921, 2008.

[8] W. Aniszewski, T. Ménard, and M. Marek. Volume of fluid (VOF) type advection methods in two-phase flow: A comparative study. *Computers & Fluids*, 97:52–73, 2014.

[9] S. Tanguy and A. Berlemont. Application of a level set method for simulation of droplet collisions. *International Journal of Multiphase Flow*, 31:1015–1035, 2005.

[10] O. Desjardins, V. Moureau, and H. Pitsch. An accurate conservative level set/ghost fluid method for simulating turbulent atomization. *Journal of Computational Physics*, 227:8395–8416, 2008.

[11] M. Herrmann. A balanced force refined level set grid method for two-phase flows on unstructured flow solver grids. *Journal of Computational Physics*, 227:2674–2706, 2008.

[12] M. Sussman and E. G. Puckett. A coupled level set and volume-of-fluid method for computing 3D and axisymmetric incompressible two-phase flows. *Journal of Computational Physics*, 162,:301–337, 2000.

[13] V. Le Chenadec and H. Pitsch. A 3D unsplit forward/backward volume-of-fluid approach and coupling to the level set method. *Journal of Computational Physics*, 233:10–33, 2013.

[14] G. Vaudor, T. Ménard, W. Aniszewski, M. Doring, and A. Berlemont. A consistent mass and momentum flux computation method for two phase flows. application to atomization process. *Computers and Fluids*, 152:204–216, 2017.

[15] M. Owkes and O. Desjardins. A mass and momentum conserving unsplit semi-lagrangian framework for simulating multiphase flows. *Journal of Computational Physics*, 332:21–46, 2017.

[16] V. Dyadechko and M. Shashkov. Reconstruction of multi-material interfaces from moment data. *Journal of Computational Physics*, 227:5361–5384, 2008.

[17] M. Jemison, E. Loch, M. Sussman, M. Shashkov, M. Arienti, M. Ohta, and Y. Wang. A coupled level set-moment of fluid method for incompressible two-phase flows. *Journal of Scientific Computing*, 54:454–491, 2013.

[18] G. Li, Y. Lian, Y. Guo, M. Jemison, M. Sussman, T. Helms, and M. Arienti. Incompressible multiphase flow and encapsulation simulations using the moment-of-fluid method. *International Journal for Numerical Methods in Fluids*, 79:456–490, 2015.

[19] G. D. Weymouth and D. K.-P. Yue. Conservative volume-of-fluid method for free-surface simulations on cartesian-grids. *Journal of Computational Physics*, 229:2853–2865, 2010.

[20] S. Bnà, A. Cervone, V. Le Chenadec, and M. Sandro. Review of split and unsplit geometric advection algorithms. In *11th International Conference of Numerical Analysis and Applied Mathematics 2013, ICNAAM 2013, Rhodes, Greece*, volume 1558, pages 875–878, 2013.

[21] J. Cousin, T. Ménard, A. Berlemont, and S. Grout. Primary breakup simulation of a liquid jet discharged by a low-pressure compound nozzle. *Computers & Fluids*, 63:165–173, 2012.

[22] B. Duret, G. Luret, J. Réveillon, T. Ménard, A. Berlemont, and F.-X. Demoulin. DNS analysis of turbulent mixing in two-phase flows. *International Journal of Multiphase Flow*, 40:93–105, 2012.

[23] M. Sussman, K. M. Smith, M. Y. Hussaini, M. Ohta, and R. Zhi-Wei. A sharp interface method for incompressible two-phase flows. *Journal of Computational Physics*, 221(2):469–505, February 2007.

[24] R. Fedkiw, T. Aslam, B. Merriman, and S. Osher. A Non-oscillatory Eulerian Approach to Interfaces in Multimaterial Flows (the Ghost Fluid Method). *Journal of Computational Physics*, 152(2):457–492, July 1999.

[25] J. López, J. Hernández, P. Gómez, and F. Faura. A volume of fluid method based on multidimensional advection and spline interface reconstruction. *Journal of Computational Physics*, 195(2):718–742, April 2004.

[26] O. Desjardins and H. Pitsch. A spectrally refined interface approach for simulating multiphase flows. *Journal of Computational Physics*, 228:1658–1677, 2009.

[27] P. K. Smolarkiewicz. The multi-dimensional crowley advection scheme. *Monthly Weather Review*, 110:1968–1983, December 1982.

[28] D. Enright, R. Fedkiw, J. Ferziger, and I. Mitchell. A hybrid particle level set method for improved interface capturing. *Journal of Computational Physics*, 183(1):83–116, November 2002.

[29] R. J. LeVeque. High-resolution conservative algorithms for advection in incompressible flow. *SIAM Journal on Numerical Analysis*, 33(2):627–665, 1996.
[30] G. Vaudor. *Atomisation assistée par un cisaillement de l' écoulement gazeux. Développement et validation.* PhD thesis, University de Rouen Normandie, April 2015.
[31] A. Prosperetti. Viscous effects on small–amplitude surface waves. *Physics of Fluids*, 19:195–203, 1976.
[32] R. Menikoff, R. C. Mjolsness, D. H. Sharp, C. Zemach, and B. J. Doyle. Initial value problem for Rayleigh–Taylor instability of viscous fluids. *Physics of Fluids*, 21:1674–1687, 1978.
[33] A. Prosperetti. Motion of two superposed viscous fluids. *Physics of Fluids*, 24:1217–1223, 1981.